

Adversarial Detection without Model Information

Abhishek Moitra, Youngeun Kim, and Priyadarshini Panda
Department of Electrical Engineering
Yale University
New Haven, CT, USA

{abhishek.moitra,youngeun.kim, priya.panda}@yale.edu

Abstract

Most prior state-of-the-art adversarial detection works assume that the underlying vulnerable model is accessible, i.e., the model can be trained or its outputs are visible. However, this is not a practical assumption due to factors like model encryption, model information leakage and so on. In this work, we propose a model independent adversarial detection method using a simple energy function to distinguish between adversarial and natural inputs. We train a standalone detector independent of the underlying model, with sequential layer-wise training to increase the energy separation corresponding to natural and adversarial inputs. With this, we perform energy distribution-based adversarial detection. Our method achieves state-of-the-art detection performance (ROC-AUC > 0.9) across a wide range of gradient, score and decision-based adversarial attacks on CIFAR10, CIFAR100 and TinyImagenet datasets. Compared to prior approaches, our method requires ~ 10 - $100x$ less number of operations and parameters for adversarial detection. Further, we show that our detection method is transferable across different datasets and adversarial attacks. For reproducibility, we provide code in the supplementary material.

1. Introduction

Deep Neural Networks (DNNs) have achieved state-of-the-art performance in many real-life applications. However, they are vulnerable to adversarial attacks [2, 24]. Adversarial images are created by adding small crafted noise to natural images that can easily fool a DNN to make high confidence mis-classifications. Therefore, there is a need to improve the robustness of DNNs against adversarial attacks.

Previous adversarial defense works have focused on two broad approaches: 1) Adversarial classification- by employing adversarial training [21], input transformation [13], randomization [27] among others to improve classification accuracy of models on adversarial inputs; 2) Adversarial de-

tection works- employ “detector” networks trained to identify adversarial and natural inputs in a system [22, 29, 30]. In this work, we narrow down the scope to adversarial detection.

Prior works on adversarial detection have achieved state-of-the-art performance on several adversarial attacks. However, **they assume that the underlying vulnerable model is accessible**, i.e., either the parameters of the vulnerable model can be trained or the outputs of the model are visible. However, we argue that model accessibility is not a practical assumption. A vulnerable model might be difficult to access because of several reasons: 1) model encryption 2) model information leakage leading to threat of white-box attacks [18, 21] 3) cost overhead of model redaction and re-deployment [4]. Therefore, there is a need for target model independent adversarial defense approaches. Note, in this work, we refer to the underlying vulnerable model that requires hardening against adversarial attacks as the *target model*.

In this work, we propose an adversarial detection method (shown in Fig. 1) that does not require access to the target model, i.e., training and outputs of the target model. As seen in Fig. 1a, the target model (M_T) is trained on the natural inputs x_{nat} . Hence, it is vulnerable to adversarial inputs x_{adv} . To provide adversarial robustness to the target model, we augment an adversarial detector to eliminate adversarial inputs from being sent to the target model. The adversarial detector network \mathcal{D} is trained using the dataset $[x_{nat}, x'_{adv}]$. Here x'_{adv} is a set of adversarial inputs created using x_{nat} and the source model M_S . The *source model* can have an arbitrary network architecture and is trained with standard backpropagation on x_{nat} . Note, training of M_S , \mathcal{D} and x'_{adv} generation does not require access to the target model. It is evident that for training the detector, we require access to the dataset x_{nat} .

We propose a simple *energy function* based on the summation of feature outputs in the detector network. As adversaries are created by adding noise to natural data, we find that the energy values corresponding to natural and ad-

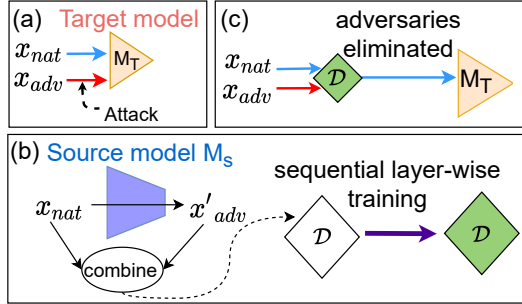


Figure 1. a) Our proposed approach assumes that the vulnerable target model trained on natural dataset x_{nat} is inaccessible for adversarial detection. b) We train a separate source model on x_{nat} and generate adversarial data x'_{adv} with the source model. Using $[x_{nat}, x'_{adv}]$, we train a small detector network. This is done independent of the target model knowledge. c) The adversarial detector detects and eliminates adversarial data from attacking the target model

versarial data are different. However, the difference is not sufficient to perform reliable adversarial detection. In order to increase the energy separation, we use a sequential layer-wise training using an energy separation-based loss function that maximizes the distance between natural and adversarial energies. We show that our proposed adversarial detector transfers across a wide range of adversarial attacks proposed in recent literature [3, 7, 8, 18, 21]. Further, the detector is transferable across different datasets. For example, a detector constructed using CIFAR100 data can detect adversarial attacks on target models trained on CIFAR10 and TinyImagenet datasets. To the best of our knowledge, the transferability of adversarial detection across different datasets has not been demonstrated in prior works. Table 1 compares our work with prior adversarial detection works.

In summary, the contributions of our work are:

- We propose a simple and light-weight energy metric to distinguish between clean and adversarial inputs. To perform adversarial detection, we maximize the energy distance between them using an energy separation-based objective function and a sequential layer-wise training approach. Our adversarial detection approach does not require any access to the target model parameters or outputs.
- We perform extensive experiments on benchmark datasets like CIFAR10, CIFAR100, and TinyImagenet with state-of-the-art gradient-based [18, 21], score-based [8] and decision-based [7] adversarial attacks. We find our approach yields state-of-the-art detection across different adversarial attacks and datasets. Further, we find that the detector is transferable across different datasets. Using transferability, a detector trained

Table 1. Table showing the key differences between our proposed and prior adversarial detection works (✓: addressed / ✗: not addressed).

Work	Transferability		Type of target model access
	Attacks	Datasets	
Metzen et al. [22], Yin et al. [30], Sterneck et al. [25]	✓	✗	intermediate activations required
Moitra et al. [23], Xu et al. [29], Grosse et al. [12]	✓	✗	model training required
Huang et al. [15],	✓	✗	model outputs required
Ours	✓	✓	No access required

on one dataset can be reused to detect adversaries created on another dataset.

- Through our ablation studies, we find that the error amplification effect discussed in [20] aids in improving the energy separation in the detector network. Consequently, we find that a higher Lipschitz constant [6] enables better adversarial detection.

2. Background

2.1. Adversarial Attacks

In this work, we consider three different kinds of adversarial attacks. Here, we discuss those attacks in detail.

Gradient-based attacks: These attacks require gradients of the input to craft adversaries. The Fast Gradient Sign Method (FGSM) is a simple one-step adversarial attack proposed in [18]. Several works have shown that FGSM attack can be made stronger with momentum (MIFGSM) [10], random initialization (FFGSM) [26], and input diversification (DIFGSM) [28]. In contrast, the Basic Iterative Method (BIM) is an iterative attack proposed in [18]. The BIM attack with random restarts is called the Projected Gradient Descent (PGD) attack [21]. A targeted version of the PGD attack (TPGD) [31] can fool the model into mis-classifying a data as a desired class. Other multi-step attacks like Carlini-Wagner (C&W) [5] and PGD-L2 [21] are crafted by computing the L2 Norm distance between the adversary and the natural images.

Score-based attacks: Score-based attacks do not require input gradients to craft adversaries. Square attack (Square) [3] uses multiple queries to perturb randomly selected square regions in the input. Other score-based attacks like the AutoAttack and Auto-PGD (APGD) craft adversaries by automatically choosing the optimal attack parameters [8].

Decision-based attacks: These attacks craft adversaries based on the decision outputs of a model. The Fast Adaptive Boundary (FAB) [7] attack finds the minimum perturbation required to perform a mis-classification. The Gaussian Noise (GN) attack is created by adding gaussian noise to the input.

2.2. Performance Metrics for Adversarial Detection

To evaluate the adversarial detection performance, we use three metrics: ROC-AUC, Accuracy and Error.

Area Under the ROC Curve (ROC-AUC): The area under the ROC curve, compares the True Positive Rate (TPR) and the False Positive Rate (FPR) of a classifier. A high ROC-AUC score signifies a good classifier [30].

Accuracy and Error: In this work, *Accuracy* is defined as the fraction of natural inputs that are correctly classified by the target model and not rejected by the adversarial detector. While, *Error* is defined as the fraction of adversarial inputs that are classified incorrectly by the target model and not rejected by the detector. Thus, high accuracy and low error is desirable.

3. Related Works

3.1. Adversarial Classification

Here, the objective is to improve the adversarial classification accuracy of a vulnerable model. Guo et al. proposed input feature transformation using JPEG compression followed by training on compressed feature space to improve the classification performance of the target model. Madry et al. [21] proposed adversarial training in which a target model is trained on adversarial and clean data to improve the adversarial and clean classification performance. Following this, several works have used noise injection into parameters [14] and ensemble adversarial training to harden the target model against a wide range of attacks. Lin et al. [20] showed that adversarial classification can be improved by reducing the error amplification in a network. Hence, they used adversarial training with regularization to constrain the Lipschitz constant of the network to less than unity. In our work, we do not improve the adversarial classification accuracy of the target model. Rather, we focus on adversarial detection to distinguish adversarial data from natural ones.

3.2. Adversarial Detection

3.2.1 Works requiring target model training

The following works require training of the target model to perform adversarial detection. Xu et al. [29] propose a method that uses outputs of multiple target models to estimate the difference between natural and adversarial data. Here, the target models are trained on natural inputs with different feature squeezing techniques at the inputs. Moitra et al. [23] uses the features from the first layer of the underlying model to perform adversarial detection. In particular, they perform adversarial detection using hardware signatures in DNN accelerators. Further, several recent works like [11] have shown that adversarial and natural data have different data distributions. While Grosse et al. [12] train

the target model with an additional class label indicating adversarial data, Gong et al. [11] train a separate binary classifier on the natural and adversarial data generated from the target model to perform adversarial detection. Lee et al. [19] use a metric called the *Mahalanobis distance* classifier to train the target model. The Mahalanobis distance is used to distinguish natural from adversarial data.

3.2.2 Works requiring target model outputs

These works show that adversarial and natural inputs can be distinguished based on the intermediate features of the target model. Metzen et al. [22] and Sterneck et al. [25] use the intermediate features to train a simple binary classifier for adversarial detection. While Metzen et al. [22] use a heuristic-based method to determine the point of attachment of the detector with the target model, Sterneck et al. [25] use a structured metric called adversarial noise sensitivity to do the same. Similarly, Yin et al. [30] use asymmetric adversarial training to train detectors on the intermediate features of the target model for adversarial detection. Another work by Ahuja et al. [1] use the data distributions from the intermediate layers in the target model and Gaussian mixture models to perform adversarial detection. Further, Huang et al. [15] use the confidence scores from the target model to estimate the *relative score difference* corresponding to the clean and the adversarial input to perform adversarial detection. Further, they also recommend target model training on noisy data to improve the adversarial detection performance.

Evidently, prior works discussed in the Section 3.2.1 and Section 3.2.2 require training or the outputs of the target model for adversarial detection. In contrast, our work is focused towards performing adversarial detection without accessing the target model.

4. Sequential Layer-wise Training and Analysis

In this work, we define a simple energy function for layer l , \mathcal{E}^l shown in the Eq. 1. The energy is defined as the average magnitude of the feature outputs in a particular layer l with outputs $Z_l^{c,h,w}$. Here c , h , and w are the number of output channels, height and width, respectively of the feature outputs in the layer l . In sequential layer-wise training, we train the detector network to maximize the energy separation between \mathcal{E}_{nat} and \mathcal{E}_{adv} . Here, \mathcal{E}_{nat} and \mathcal{E}_{adv} are the energies corresponding to natural and adversarial inputs, respectively. Note, the energy separation is the difference between the mean values of \mathcal{E}_{nat} and \mathcal{E}_{adv} distributions.

$$\mathcal{E}^l = \frac{1}{chw} \sum_{i=1}^c \sum_{j=1}^h \sum_{k=1}^w |Z_l^{i,j,k}|. \quad (1)$$

Training objective: We train the detector using the following objective function:

$$\max_{\theta} \|\mathcal{E}_{nat}^l - \mathcal{E}_{adv}^l\|, \quad (2)$$

corresponding to any layer l . Here, θ denotes the parameters of the detector network. In order to achieve this, we design an energy separation-based loss function that minimizes the energy distances between \mathcal{E}_{nat}^l (\mathcal{E}_{adv}^l) and λ_n (λ_a). Here, λ_n and λ_a are hyper-parameters denoting the desired natural and adversarial energies, respectively. An indicator variable y has the value of 1 or 0 for natural and adversarial inputs, respectively.

$$\mathcal{L} = y \mathcal{L}_{MSE}(\mathcal{E}_{nat}^l, \lambda_n) + (1 - y) \mathcal{L}_{MSE}(\mathcal{E}_{adv}^l, \lambda_a). \quad (3)$$

Note, our training objective is loosely based on the current signature separation in recent work [23]. We would like to highlight that [23] focuses on modifying the target model’s layers to perform adversary detection. In contrast, we train the detector independently that enables high detection scores along with transferability across multiple datasets and attacks.

Training dataset generation and s_{nat} : The training dataset for the detector contains equal number of natural (x_{nat}) and adversarial data (x'_{adv}). x'_{adv} is created using a source model with arbitrary network architecture trained on x_{nat} using the Stochastic Gradient Descent (SGD) algorithm. A sample dataset s_{nat} is created by random selection of 10k data samples from the natural dataset x_{nat} that is later used in the detector.

Algorithm 1: Sequential layer-wise training

input : n layered detector (\mathcal{D}), x_{nat} , x'_{adv} , s_{nat}
output: n layered trained detector \mathcal{D}_T , \mathcal{E}_{Th}
while $i \leq n$ **do**
 while $j \leq epochs$ **do**
 Freeze layers $[0, i-1]$;
 Compute \mathcal{E}_{nat}^i and \mathcal{E}_{adv}^i ;
 Optimize layer i using loss Eq. 3;
 end
end
Generate distribution $\mathcal{E}_{s_{nat}}$ with s_{nat} and \mathcal{D}_T ;
 $\mathcal{E}_{Th} \leftarrow K^{th}$ percentile of $\mathcal{E}_{s_{nat}}$;

Sequential layer-wise training methodology: Algorithm 1 shows the sequential layer-wise training approach. It begins with a randomly initialized n layered detector, where, n is a hyper-parameter. The training is carried out in multiple stages where in each stage i , layers $[0, i-1]$ are frozen and layer i is optimized for energy distance maximization. During each stage, the loss shown in Eq. 3 is

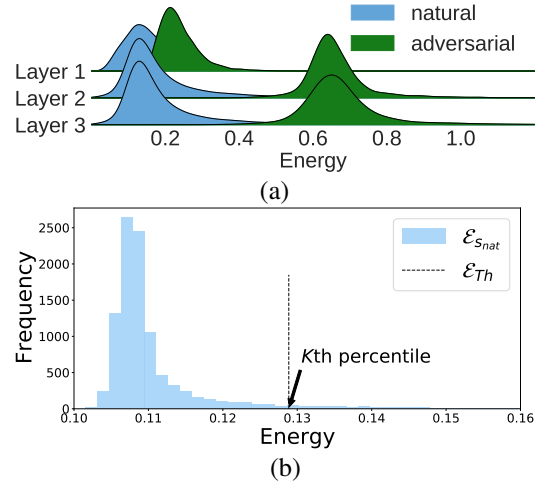


Figure 2. a) The separation between the clean and adversarial energy distributions increase with with each layer as the sequential layer-wise training proceeds. The energy distributions correspond to natural and PGD [4,2,10] adversarial data. b) The value of \mathcal{E}_{Th} is set as the K th percentile value of the $\mathcal{E}_{s_{nat}}$ distribution.

computed using \mathcal{E}_{nat}^i and \mathcal{E}_{adv}^i based on the i th layer outputs. As layers $[0, i-1]$ are frozen, the energy separation obtained after layer $i-1$ is preserved. Thus, training the i th layer further increases the energy separation. Fig. 2a shows the energy separation between \mathcal{E}_{nat} and \mathcal{E}_{adv} obtained after each layer of a three-layered detector trained on the CIFAR100 dataset in the layer-wise manner. The adversarial inputs correspond to PGD [4,2,10]¹ attack on the testset of the CIFAR100 dataset. It can be seen that the energy separation increases with each layer in the detector. The increasing separation significantly improves the detection of weak attacks² (like PGD [4,2,10]), that may go undetected at early layers due to low energy separation. In the final layer, such attacks can be detected successfully.

Next, we use \mathcal{D}_T to create the energy distribution for the sample natural (s_{nat}) dataset as shown in Fig. 2b. The value of \mathcal{E}_{Th} is chosen as the K th percentile of the $\mathcal{E}_{s_{nat}}$ distribution. All energy values greater than \mathcal{E}_{Th} are classified as adversarial inputs and vice-versa. In Section 4.4, we show the effect of choosing K on the performance of the detector.

4.1. Lipschitz Constant and Energy Distance

The Lipschitz constant has been associated with the error amplification effect in a neural network [20]. The Lipschitz constant of a feed-forward function f_l for any layer l , can

¹PGD[4,2,10]= PGD with parameters $\epsilon: 4/255, \alpha: 2/255, steps: 10$.

²Weak attacks have smaller ϵ values compared to stronger attacks

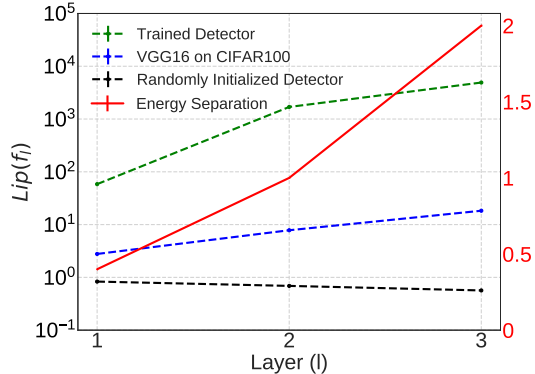


Figure 3. Comparison of Lipschitz constant of feed-forward function ($Lip(f_i)$) for three different networks. Note, only first three layers of the VGG16 network have been shown. It is observed that $Lip(f_i)$ increases exponentially as the energy separation (in red) between \mathcal{E}_{nat} and \mathcal{E}_{adv} increases. Compared to the detector, rise in $Lip(f_i)$ is negligible for the other two networks.

be expressed as follows:

$$Lip(f_l) \leq \prod_{i=1}^l Lip(\phi_i). \quad (4)$$

where ϕ can be a linear, convolutional, max pool layer or an activation layer.

Fig. 3 shows the $Lip(f_i)$ values for three different networks: i) A randomly initialized 3-layered detector network, ii) the 3-layered detector after layer-wise training on the CIFAR100 dataset, and iii) a VGG16 network trained on the CIFAR100 dataset using SGD. Interestingly, we observe that the value of $Lip(f_i)$ exponentially rises as the energy separation between \mathcal{E}_{nat}^l and \mathcal{E}_{adv}^l increases. This suggests that the layer-wise training increases the error amplification factor in the detector network.

In prior works that minimize the adversarial perturbations in a network [6, 20], it has been shown that a lower Lipschitz constant helps in reducing the adversarial perturbations and thus increase adversarial robustness. *However, in this work, we show that a higher Lipschitz constant is associated with higher energy separation and thus, higher adversarial detection.*

4.2. Effect of Batch-Normalization

Table 2. Table showing detectors with and without BN layers

With BN	Conv2D 3x8	BN	ReLU	Conv2D 8x16	BN	ReLU	Conv2D 16x32
Without BN	Conv2D 3x8	ReLU	Conv2D 8x16	ReLU	Conv2D 16x32		

This section empirically shows the effect of including batch normalization (BN) layers on the sequential layer-

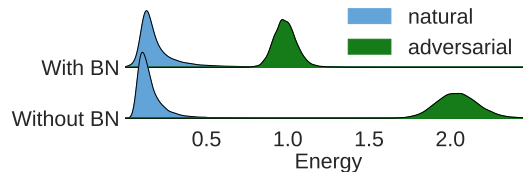


Figure 4. Energy distributions obtained at the final convolutional layer of two detector networks.

wise training performance. We consider two detector networks: *Detector with BN layers* and a *Detector without BN layers*. The configurations are shown in Table 2. Sequential layer-wise training is performed on both the detectors with identical hyper-parameters. We plot the \mathcal{E}_{nat} and \mathcal{E}_{adv} distributions at the end of the final layer. *Interestingly, as seen in Fig. 4, the detector without the BN layers achieves a higher energy separation (and higher adversarial detection) than the detector with BN layers.* For all our future experiments, we use a detector network without BN layers.

4.3. Effect of Architecture on Energy separation

Table 3. Table showing detector architectures with varying widths.

Detector	L1	L2	L3	L4	L5
Detector A	Conv2D 3x64	ReLU	Conv2D 64x128	ReLU	Conv2D 128x256
Detector B	Conv2D 3x32	ReLU	Conv2D 32x64	ReLU	Conv2D 64x128
Detector C	Conv2D 3x8	ReLU	Conv2D 8x16	ReLU	Conv2D 16x32

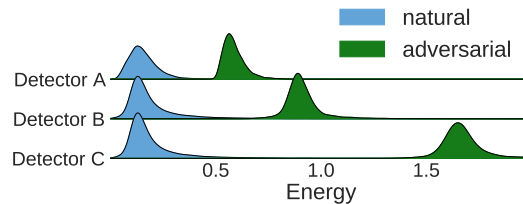


Figure 5. The clean and adversarial energy distributions corresponding to the different network architectures shown in Table 3.

To analyse the effect of detector model architecture on energy separation, we consider 3 different detector model architectures shown in Table 3. All three detectors have the same depth but different width of the convolution layers. All the models undergo sequential layer-wise training with the same hyper-parameter values. Interestingly, as seen in Fig. 5, the detector with narrow convolutional layers achieves higher energy separation in the final layer compared to the wider networks. *Consequently, light-weight detectors improve the adversarial detection performance.*

Table 4. Table showing the effect of choosing K on the detection of different PGD attacks on the CIFAR100 dataset.

Percentile (K)	PGD [4,2,10]	PGD [8,4,10]	PGD [16,4,10]
90	0.95	0.96	0.96
95	0.92	0.98	0.98
97	0.8	0.98	0.99

4.4. Effect of Choosing the Threshold Percentile

In this section, we show how adversarial detection is affected by the choice of \mathcal{E}_{Th} . The value \mathcal{E}_{Th} is chosen as the K^{th} percentile of the $\mathcal{E}_{s_{nat}}$ distribution. Table 4 shows the ROC-AUC scores corresponding to strong (PGD [16,4,10], PGD [8,4,10]) and weak (PGD [4,2,10]) adversarial attacks for three different cases: 1) $K=90$ 2) $K=95$ and 3) $K=97$. Adversarial data is generated using the source model and s_{nat} data. Clearly, choosing $K=95$ provides an overall high ROC-AUC score across all attacks. This is because weak attacks have a smaller energy separation compared to stronger attacks (see supplementary material for more details). For uniformity, in all the following experiments in the paper, \mathcal{E}_{Th} is chosen as the 95th percentile of the $\mathcal{E}_{s_{nat}}$ distribution.

5. Results

5.1. Datasets

We use three different image datasets for our experiments: CIFAR10 [17], CIFAR100 [17], and TinyImagenet [9]. The training data is pre-processed with the following techniques: random cropping of window size 32 for CIFAR10 and CIFAR100 while 64 for TinyImagenet, input padding, and random horizontal flip. For testing, the CIFAR10 and CIFAR100 data is resized to 32x32 while the TinyImagenet inputs are resized to 64x64 pixels. Both the training and testing data are scaled in the range [0,1] and input data normalization is *not* applied in any of the experiments. For generating adversarial attacks, we use the torchattacks library [16].

5.2. Experimental Setup

1. *Target Models*: In all our experiments, the target models have a VGG19 network architecture trained on the the natural data of CIFAR10, CIFAR100 and TinyImagenet datasets using the SGD algorithm.
2. *Source Models*: For all experiments (except in Section 5.4), the source models have a VGG16 network architecture irrespective of the dataset used. The source models are trained on the natural data using the SGD algorithm.
3. *Detector*: For the CIFAR10 and CIFAR100 datasets,

Table 5. Table showing the detection performance across white-box (WB) and black-box (BB) attacks.

Architecture	MobileNetV2 (BB)	ReNet18 (BB)	VGG19 (WB)
APGD [8]	0.81	0.82	0.8
AutoAttack [8]	0.80	0.79	0.81
BIM [18]	0.98	0.97	0.985
C&W [5]	0.8	0.8	0.81
DIFGSM [28]	0.97	0.98	0.98
FAB [7]	0.505	0.50	0.51
FFGSM [26]	0.98	0.98	0.98
FGSM [18]	0.985	0.97	0.97
GN	0.98	0.975	0.98
MIFGSM [10]	0.98	0.98	0.98
PGD8 [21]	0.98	0.98	0.98
PGD-L2 [21]	0.8	0.82	0.8
PGD4 [21]	0.95	0.94	0.96
Square [3]	0.81	0.81	0.81
TPGD [31]	0.98	0.98	0.98

we use a three-layered detector ($n=3$). The first layer is a convolutional layer with 3-input channels and 8-output channels. The second convolutional layer has 8-input channels and 16-output channels. The third convolutional layer has 16-input channels and 32-output channels. The detector for the TinyImagenet dataset has an additional MaxPool layer after the first convolutional layer. The training dataset contains equal number of natural and PGD[8,4,10] data. The learning rate and hyper-parameters, λ_n and λ_a for stage 1, stage 2 and stage 3 are (0.005, 0.1, 0.6), (0.001, 0.1, 1) and (0.001, 0.1, 2), respectively. Each stage of the training consists of 500 epochs. Note, due to the small detector architecture, training time is in the order of few hours. The training is carried out using the SGD algorithm with [momentum=0.6 and weight decay= 5×10^{-4}]. All the experiments are carried out on the Pytorch 1.4.0 framework on a single Nvidia RTX2080ti GPU.

5.3. Performance on Different Adversarial Attacks

We test the layer-wise trained detector on a wide range of state-of-the-art adversarial attacks : gradient-based [5, 10, 18, 21, 26], score-based [3, 8] and decision-based attacks [7]. Fig. 6 shows energy distribution, ROC-AUC and error values for different attacks on the CIFAR100 dataset. The detailed description and hyper-parameters used to generate the adversarial attacks, can found in the supplementary material. The \mathcal{E}_{Th} is marked by a dotted line on the energy axis of each plot. Note, the attacks are crafted using the source model used to create x'_{adv} explained in Section 4. We find that the detector can detect numerous gradient-based (FGSM, PGD, FFGSM, TPGD, among others) and gaussian noise attacks. This is marked by a large energy separation between \mathcal{E}_{nat} (blue) and \mathcal{E}_{adv} (green) distributions as seen in Fig. 6a-j and 6n. This leads to negligible error values for these attacks. Interestingly, we find that the

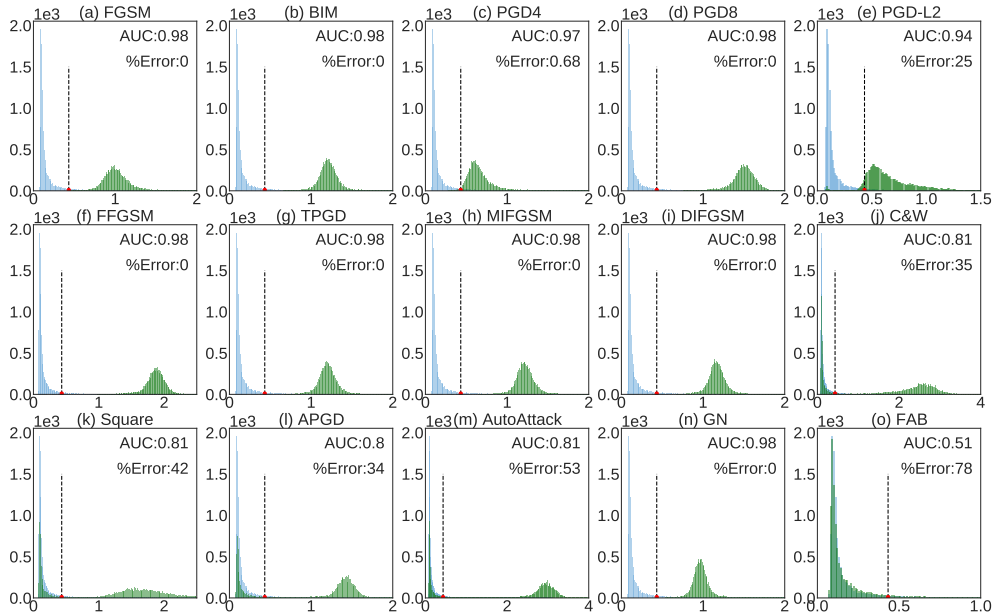


Figure 6. Energy distributions, ROC-AUC, error and accuracy values across various gradient-based, score-based and decision-based adversarial attacks created using the CIFAR100 dataset. The x axis of the distributions denote the energy values.

detector trained on gradient-based adversarial attack (PGD) can detect score-based adversarial attacks like the Square, APGD and Autoattack shown in Fig. 6k-m. However, the ROC-AUC scores are slightly low as the natural and adversarial energy distributions have a partial overlap. This leads to a rise in the error value. Similar results are obtained with the CIFAR10 and the TinyImagenet datasets shown in the supplementary material.

The detector however fails to detect decision-based attacks like the FAB attack shown in Fig. 6o. This is because FAB attacks add minimal perturbations to the natural input which does not change the \mathcal{E}_{adv} value significantly. Consequently, a high error value is observed. Further, due to the detector, the top 5 percentile natural data is misclassified as adversarial. This leads to a drop in the accuracy value to 50% compared to the baseline accuracy value of 54% achieved on the target model without detector.

5.4. Agnostic to White-Box and Black-Box Attacks

We test the robustness of the detector under different white-box and black-box attack scenarios for the CIFAR100 dataset. For the white-box scenario, we assume that the parameters of the target model (VGG19) are known to the attacker. While for the black-box scenario, we assume that the target model parameters are unknown. We generate black-box adversarial attacks using two different models: ResNet18 and MobileNet_V2 trained on the CIFAR100 dataset. Table 5 shows the ROC-AUC scores under different white-box and black-box adversarial attacks. *Evidently, the*

performance of the detector remains unperturbed irrespective of the model used for crafting the adversarial attacks.

5.5. Comparison with Prior Works

Table 6 compares the performance and cost-effectiveness of our proposed method with prior state-of-the-art adversarial detection works. Metzen et al. [22], Yin et al. [30], and Sterneck et al. [25] train neural network-based detectors on the intermediate features of the target model for adversarial detection. On the other hand, Xu et al. [29] and Moitra et al. [23] train the target model for improving the adversarial detectability. Gong et al. [11] propose a binary classifier approach that requires adversarial data generated using the target model for training. In comparison to all the prior state-of-the-art works, our method is target model independent. In addition, we achieve comparable or higher adversarial detection. The striking feature of our approach is the energy-based separation and layer-wise training that generalizes well to both weak and strong adversarial attacks. Further, unlike [25], our approach is agnostic to white-box and black-box attacks.

Computational overhead: Besides high adversarial detection, our method requires $\sim 10 \times -100 \times$ less number of operations and parameters for adversarial detection compared to works [11, 22, 25, 29, 30]. Although we require more parameters compared to [23], the number of computations in our detection is significantly less. This makes our approach suitable for deployment in resource constrained computing systems. Note, the number of operations is estimated as to-

Table 6. Table comparing the performance of our method with prior state-of-the-art adversarial detection works.

Work	Dataset	Weak Attacks		Strong Attacks		Number of Operations	Number of Parameters
		FGSM ϵ : 4/255	PGD ϵ : 4/255	FGSM ϵ : 16/255	PGD ϵ : 16/255		
Metzen et al. [22]	CIFAR10	1	0.96	–	–	$\sim 500k$	$\sim 1.4M$
Yin et al. [30]	CIFAR10	–	–	–	0.953	$\sim 213k$	$\sim 6.04M$
Moitra et al. [23]	CIFAR10	–	0.89	0.98	0.895	$\sim 1.7k$	$\sim 589k$
Sterneck et al. [25]	CIFAR10	–	0.998	–	1	$\sim 525k$	$\sim 4.7M$
Xu et al. [29]	CIFAR10	0.208	0.505	–	–	$\sim 10G$	$\sim 10G$
Gong et al. [11]	CIFAR10	0.003	–	1	–	$\sim 64k$	$\sim 477k$
Ours	CIFAR10	0.96	0.985	0.99	0.99	$\sim 5.9k$	$\sim 500k$
Sterneck et al. [25]	CIFAR100	–	–	–	1	$\sim 525k$	$\sim 4.7M$
Moitra et al. [23]	CIFAR100	–	–	0.98	0.99	$\sim 1.7k$	$\sim 589k$
Ours	CIFAR100	0.96	0.97	0.985	0.985	$\sim 5.9k$	$\sim 500k$
Moitra et al. [23]	TinyImagenet	–	–	0.84	0.65	$\sim 1.7k$	$\sim 589k$
Ours	TinyImagenet	0.96	0.97	0.985	0.985	$\sim 5.9k$	$\sim 147k$

Table 7. Table showing transferability of adversarial detection from a source dataset to a target dataset.

Source Dataset	Target Dataset	PGD [4,2,10] [21]	PGD [8,4,10] [21]	APGD [8]	AutoAttack [8]	C&W [5]	GN	PGD-L2 [21]	Square [3]
TinyImagenet	CIFAR10	0.55	0.98	0.92	0.92	0.92	0.98	0.98	0.91
TinyImagenet	CIFAR100	0.53	0.98	0.8	0.81	0.81	0.98	0.97	0.81
CIFAR100	CIFAR10	0.55	0.98	0.91	0.92	0.92	0.98	0.98	0.91
CIFAR100	TinyImagenet	0.52	0.98	0.68	0.74	0.74	0.98	0.98	0.74

tal number of dot-product computations across all layers.

5.6. Effect of Quantization on Performance

Table 8. Table showing the effect of quantization on the detection performance of a CIFAR100 trained detector.

Quantization	PGD [4,2,10]	PGD [8,4,10]	PGD [16,4,10]
32-bit	0.96	0.98	0.99
16-bit	0.96	0.98	0.99
8-bit	0.94	0.97	0.985
4-bit	0.5	0.505	0.505

In this section, we discuss how the detection is affected by the quantization of the detector network. We perform experiments on the CIFAR100 dataset. The detector is trained using sequential layer-wise training with quantization. The model weights are quantized to 16-bit, 8-bit and 4-bit values. Table 8 shows the ROC-AUC scores achieved across different strengths of PGD attacks corresponding to different quantization. For 16-bit and 8-bit quantization, the detector shows similar detection as a 32-bit full precision detector. However, at 4-bit quantization, adversarial detection is drastically reduced.

5.7. Transferability Across Datasets

In this section, we explore the following question: *Can a detector trained on dataset A be used to detect adversaries from another dataset B?* We refer to “dataset A” as the

source dataset and “dataset B”, the *target dataset*.

Methodology: The detector network is trained on a source dataset using the sequential layer-wise training explained in Section 4. After the layer-wise training, a sample dataset $s_{nat,target}$ is sampled from the target dataset. This is used to generate the $\mathcal{E}_{s_{nat,target}}$ distribution. Following this, the value of \mathcal{E}_{Th} is chosen as the 95th percentile of the $\mathcal{E}_{s_{nat,target}}$ distribution.

Experiments: We perform two experiments: 1) A detector trained on source dataset CIFAR100 and tested on target datasets- CIFAR10 and TinyImagenet 2) A detector trained on source dataset- TinyImagenet and tested on target datasets- CIFAR100 and CIFAR10. For both the experiments, we test the detector on a wide range of adversarial attacks.

Evidently, as seen in Table 7 a detector trained on the CIFAR100 dataset can detect adversarial attacks on the CIFAR10 dataset. However, it cannot detect several attacks (such as, AutoAttack, APGD among others) on TinyImagenet. Interestingly, a detector trained on the TinyImagenet dataset can detect adversarial attacks on both CIFAR10 and CIFAR100 datasets.

6. Conclusion and Limitations

In this work, we propose a target model independent energy distribution-based adversarial detection method. Our approach does not require access to the underlying vulnerable model unlike prior adversarial detection works. Further,

we achieve state-of-the-art detection performance on a wide range of adversarial attacks at an extremely small computational overhead. Moreover, we show for the first time that our method is transferable across different datasets. However, our method entails few limitations. For example, threshold energy selection is heuristic and can be improved by using more sophisticated smoothing functions. Further, our approach cannot detect decision-based adversarial attacks. This can be solved by adversarial training of target models on decision-based attacks to boost robustness.

References

- [1] Nilesh A Ahuja, Ibrahim Ndiour, Trushant Kalyanpur, and Omesh Tickoo. Probabilistic modeling of deep features for out-of-distribution and adversarial detection. *arXiv preprint arXiv:1909.11786*, 2019. 3
- [2] Naveed Akhtar and Ajmal Mian. Threat of adversarial attacks on deep learning in computer vision: A survey. *Ieee Access*, 6:14410–14430, 2018. 1
- [3] Maksym Andriushchenko, Francesco Croce, Nicolas Flammarion, and Matthias Hein. Square attack: a query-efficient black-box adversarial attack via random search. In *European Conference on Computer Vision*, pages 484–501. Springer, 2020. 2, 6, 8
- [4] Han Cai, Chuang Gan, Tianzhe Wang, Zhekai Zhang, and Song Han. Once-for-all: Train one network and specialize it for efficient deployment. *arXiv preprint arXiv:1908.09791*, 2019. 1
- [5] Nicholas Carlini and David Wagner. Towards evaluating the robustness of neural networks. In *2017 IEEE Symposium on Security and Privacy (SP)*, pages 39–57. IEEE, 2017. 2, 6, 8
- [6] Moustapha Cisse, Piotr Bojanowski, Edouard Grave, Yann Dauphin, and Nicolas Usunier. Parseval networks: Improving robustness to adversarial examples. In *International Conference on Machine Learning*, pages 854–863. PMLR, 2017. 2, 5
- [7] Francesco Croce and Matthias Hein. Minimally distorted adversarial examples with a fast adaptive boundary attack. In *International Conference on Machine Learning*, pages 2196–2205. PMLR, 2020. 2, 6
- [8] Francesco Croce and Matthias Hein. Reliable evaluation of adversarial robustness with an ensemble of diverse parameter-free attacks. In *International conference on machine learning*, pages 2206–2216. PMLR, 2020. 2, 6, 8
- [9] Jia Deng, Wei Dong, Richard Socher, Li-Jia Li, Kai Li, and Li Fei-Fei. Imagenet: A large-scale hierarchical image database. In *2009 IEEE conference on computer vision and pattern recognition*, pages 248–255. Ieee, 2009. 6
- [10] Yinpeng Dong, Fangzhou Liao, Tianyu Pang, Hang Su, Jun Zhu, Xiaolin Hu, and Jianguo Li. Boosting adversarial attacks with momentum. In *Proceedings of the IEEE conference on computer vision and pattern recognition*, pages 9185–9193, 2018. 2, 6
- [11] Zhitao Gong, Wenlu Wang, and Wei-Shinn Ku. Adversarial and clean data are not twins. *arXiv preprint arXiv:1704.04960*, 2017. 3, 7, 8
- [12] Kathrin Grosse, Praveen Manoharan, Nicolas Papernot, Michael Backes, and Patrick McDaniel. On the (statistical) detection of adversarial examples. *arXiv preprint arXiv:1702.06280*, 2017. 2, 3
- [13] Chuan Guo, Mayank Rana, Moustapha Cisse, and Laurens Van Der Maaten. Countering adversarial images using input transformations. *arXiv preprint arXiv:1711.00117*, 2017. 1
- [14] Zhezhi He, Adnan Siraj Rakin, and Deliang Fan. Parametric noise injection: Trainable randomness to improve deep neural network robustness against adversarial attack. In *Proceedings of the IEEE/CVF Conference on Computer Vision and Pattern Recognition*, pages 588–597, 2019. 3
- [15] Bo Huang, Yi Wang, and Wei Wang. Model-agnostic adversarial detection by random perturbations. In *IJCAI*, pages 4689–4696, 2019. 2, 3
- [16] Hoki Kim. Torchattacks: A pytorch repository for adversarial attacks. *arXiv preprint arXiv:2010.01950*, 2020. 6
- [17] Alex Krizhevsky, Geoffrey Hinton, et al. Learning multiple layers of features from tiny images. 2009. 6
- [18] Alexey Kurakin, Ian Goodfellow, Samy Bengio, et al. Adversarial examples in the physical world, 2016. 1, 2, 6
- [19] Kimin Lee, Kibok Lee, Honglak Lee, and Jinwoo Shin. A simple unified framework for detecting out-of-distribution samples and adversarial attacks. *Advances in neural information processing systems*, 31, 2018. 3
- [20] Ji Lin, Chuang Gan, and Song Han. Defensive quantization: When efficiency meets robustness. *arXiv preprint arXiv:1904.08444*, 2019. 2, 3, 4, 5
- [21] Aleksander Madry, Aleksandar Makelov, Ludwig Schmidt, Dimitris Tsipras, and Adrian Vladu. Towards deep learning models resistant to adversarial attacks. *arXiv preprint arXiv:1706.06083*, 2017. 1, 2, 3, 6, 8
- [22] Jan Hendrik Metzen, Tim Genewein, Volker Fischer, and Bastian Bischoff. On detecting adversarial perturbations. *arXiv preprint arXiv:1702.04267*, 2017. 1, 2, 3, 7, 8
- [23] Abhishek Moitra and Priyadarshini Panda. Detectx–adversarial input detection using current signatures in memristive xbar arrays. *IEEE Transactions on Circuits and Systems I: Regular Papers*, 2021. 2, 3, 4, 7, 8
- [24] Nicolas Papernot, Patrick McDaniel, Ian Goodfellow, Somesh Jha, Z Berkay Celik, and Ananthram Swami. Practical black-box attacks against machine learning. In *Proceedings of the 2017 ACM on Asia conference on computer and communications security*, pages 506–519, 2017. 1
- [25] Rachel Sterneck, Abhishek Moitra, and Priyadarshini Panda. Noise sensitivity-based energy efficient and robust adversary detection in neural networks. *IEEE Transactions on Computer-Aided Design of Integrated Circuits and Systems*, 2021. 2, 3, 7, 8
- [26] Eric Wong, Leslie Rice, and J Zico Kolter. Fast is better than free: Revisiting adversarial training. *arXiv preprint arXiv:2001.03994*, 2020. 2, 6
- [27] Cihang Xie, Jianyu Wang, Zhishuai Zhang, Zhou Ren, and Alan Yuille. Mitigating adversarial effects through randomization. *arXiv preprint arXiv:1711.01991*, 2017. 1
- [28] Cihang Xie, Zhishuai Zhang, Yuyin Zhou, Song Bai, Jianyu Wang, Zhou Ren, and Alan L Yuille. Improving transferabil-

- ity of adversarial examples with input diversity. In *Proceedings of the IEEE/CVF Conference on Computer Vision and Pattern Recognition*, pages 2730–2739, 2019. [2](#), [6](#)
- [29] Weilin Xu, David Evans, and Yanjun Qi. Feature squeezing: Detecting adversarial examples in deep neural networks. *arXiv preprint arXiv:1704.01155*, 2017. [1](#), [2](#), [3](#), [7](#), [8](#)
- [30] Xuwang Yin, Soheil Kolouri, and Gustavo K Rohde. Gat: Generative adversarial training for adversarial example detection and robust classification. In *International Conference on Learning Representations*, 2019. [1](#), [2](#), [3](#), [7](#), [8](#)
- [31] Hongyang Zhang, Yaodong Yu, Jiantao Jiao, Eric Xing, Laurent El Ghaoui, and Michael Jordan. Theoretically principled trade-off between robustness and accuracy. In *International Conference on Machine Learning*, pages 7472–7482. PMLR, 2019. [2](#), [6](#)